Journal of Hydrology 563 (2018) 643–656

Contents lists available at ScienceDirect

Journal of Hydrology

journal homepage: www.elsevier.com/locate/jhydrol

Research papers

Watershed- to continental-scale influences on winter stormflow in the Southern Blue Ridge Mountains

Jacob M. McDonald[a,c,*], David S. Leigh[b], C. Rhett Jackson[a]

[a] Warnell School of Forestry and Natural Resources, University of Georgia, Athens, GA 30602, USA
[b] Department of Geography, University of Georgia, Athens, GA 30602, USA
[c] Southeast Coast Network, National Park Service, Athens, GA 30605, USA

ARTICLE INFO

This manuscript was handled by Marco Borga, Editor-in-Chief, with the assistance of Shengping Wang, Associate Editor

Keywords:
Storm hydrology
Geomorphology
Continental-scale teleconnections
Soil parent material

ABSTRACT

Spatial and temporal influences on the winter (December-March) stormflow characteristics of fifteen United States Geological Survey (USGS)-gaged watersheds in the Southern Blue Ridge Mountains are identified: (1) watershed-scale differences in geomorphology; (2) continental-scale teleconnections during periods of wetness/dryness (based on the relative amount of winter precipitation over a consistent 20 year dataset); and (3) land cover in the context of soil parent material (e.g., development on alluvium/colluvium). Multiple regression was used to determine how much variance could be explained in five hydrologic variables describing the flashiness of peak flow (three original metrics), total seasonal flashiness (Richards Baker flashiness index), and the ratio of total winter stormflow to total discharge (the stormflow index). Models were constrained to three uncorrelated (|0.65|) variables to prevent overfitting to the dataset. Average-, dry-, and wet-years were subset using the z-scores for winter precipitation derived from the 4 km monthly PRISM (Parameter-elevation Relationships on Independent Slopes Model) dataset, for the period of 1986–2006. Relief, slope, and landscape connectivity explain the majority of explained variance in all five of the hydrologic variables during all time periods. During dry-, average-, and wet-years, atmospheric circulation patterns (i.e., North Atlantic Oscillation and Pacific/North American Pattern) explain more variance than total seasonal precipitation (PRISM), which is not true in the majority of the all-years models. Land cover explains only a small portion of the variance in regional stormflow and only when sub-divided based on soil parent material. Results provide a framework for connecting watershed-scale characteristics to regional- and continental-scale processes.

1. Introduction

Stormflow, or quickflow, is the non-baseflow component of a hydrograph following a precipitation event (Hewlett and Hibbert, 1967). While, precipitation and antecedent moisture conditions (intensity, duration, and spatial distribution) are the main drivers of stormflow (Bracken and Croke, 2007), the relative amount of stormflow and the flashiness of the discharge produced by a watershed is a function of watershed morphology and land cover. Generally, runoff will be greater in watersheds that have steep slopes and high relative relief (Sidle et al., 2000; Rose and Peters, 2001; Montgomery and Dietrich, 2002; Jackson et al., 2014). When antecedent moisture conditions are high, the importance of slope to runoff creation often increases because infiltrated subsurface flow is forced to flow parallel to the ground surface by a saturated zone or a relatively impermeable layer (Montgomery and Dietrich, 2002; Jackson et al., 2014). Disturbance of the 'natural' landscape can also increase the relative amount of stormflow and the flashiness of the discharge produced by a watershed (Knox, 1977; Hollis, 1979).

Disturbed and modified basins tend to have flashier and higher peak discharges (Hollis, 1975; Wright et al., 2012; Miller et al., 2004) increasing the energy available to erode channel banks and scour channel beds (Wolman, 1967; Chin, 2005). Increased sediment loadings from disturbed watersheds can have a significant economic impact due to increased reservoir sedimentation (Crowder, 1987; and Hansen and Hellerstein, 2007), decreased biodiversity (Roy et al., 2005), and a reduction in the integrity of water quality (Sutherland et al., 2002). Recent research indicates that watershed disturbance is not just about the magnitude of the disturbance but also its pattern (Jones et al., 2000; Carle et al., 2005; Alberti et al., 2007; Buchanan et al., 2013). These studies have shown that relatively small portions of a watershed (e.g., roads and agricultural drainage ditches) can have an inordinately large impact on storm discharge by increasing the hydrologic connectivity of the landscape and bypassing groundwater flow.

* Corresponding author at: Southeast Coast Network, National Park Service, Athens, GA 30605, USA.
E-mail addresses: jmcdon@uga.edu (J.M. McDonald), dleigh@uga.edu (D.S. Leigh), rjackson@warnell.uga.edu (C.R. Jackson).

https://doi.org/10.1016/j.jhydrol.2018.06.013
Received 10 November 2017; Received in revised form 30 April 2018; Accepted 6 June 2018
Available online 19 June 2018

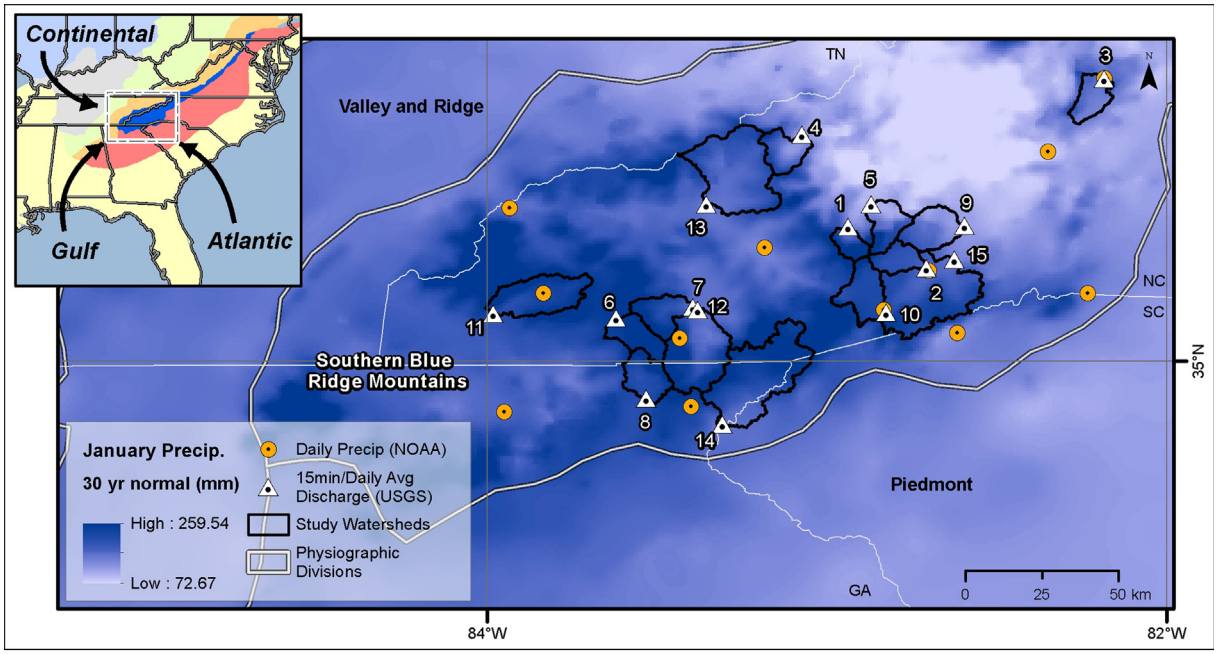

Fig. 1. 30 yr. normal January precipitation for Southern Blue Ridge Mountains (PRISM, 2014). Inset map shows the physiographic provinces of the eastern United States and the dominant storm tracks bringing precipitation to the region. On the main map, watersheds used in this study are outlined in black. Watersheds are labeled from smallest to largest based on drainage area and correspond to ID in Table 2. Triangles indicate USGS gages included in this study and orange circles show the location of daily precipitation stations in the region. (For interpretation of the references to color in this figure legend, the reader is referred to the web version of this article.)

This study focuses on water years 1986 through 2006 due to the length and completeness of the USGS gage records in the Southern Blue Ridge Mountains (Fig. 1). This research determined how low amounts of development (< 15%) and pastoral activities (< 20%) influence the amount and character of stormflow (relative to baseflow and total discharge) and the flashiness of flow in the Southern Blue Ridge Mountains (SBRM). We hypothesized that watershed morphometry would explain the majority of the variance in the amount and character of stormflow between the study watersheds. Smaller, steeper watersheds were expected to have greater amounts of stormflow and much flashier flow compared to larger watersheds with lower slopes. Additionally, we hypothesized that, especially during dry years, watersheds with greater amounts of pasture and low to moderate amounts of development in the alluvial bottomlands will have flashier flows and produce more stormflow because the landscape favors runoff over infiltration.

Research in the Upper Little Tennessee River valley of western North Carolina suggests that, at least under drought conditions, baseflow was significantly lower in pastured versus forested watersheds (Price et al., 2011). These differences in baseflow were attributed to the lower infiltration rates of compacted pasture soils versus lower bulk density forest soils (Price et al., 2010). However, examining hydrograph characteristics across this same region, Jackson et al. (2017) found that evidence of land use's influence on suspended sediment concentrations was overshadowed by regional differences in precipitation across watersheds. To account for precipitation differences across the region, the study was constrained to the winter season (December through March) when frontal systems bring more uniform distributions of precipitation (Gamble and Meentemeyer, 1997). Climatically-similar periods (average-, dry-, wet-years) were subset and analyzed separately so that the large differences in precipitation between wet and dry years would not overshadow the potential influence of land use/land cover.

Soil parent material-specific percentages of land cover were compared to general watershed-scale percentages to determine if land cover near the stream network (alluvium/colluvium) or on hillslopes (saprolite/residuum) explain more variance than the general watershed-scale percentages. Road coverages were also added to the land cover dataset to provide a metric that represents the road network-enhanced hilltop and hillslope connectivity to the stream network. Analyzing land cover percentages on spatially discrete portions of the landscape (on alluvium/colluvium or saprolite/residuum) during climatically-similar years allowed for a better understanding of how stormflow and flashiness may be affected by various scenarios of development and/or climate change.

To determine if continental-scale processes have an imprint on regional stormflow characteristics, the relative influence of indices describing the monthly modes of continental-scale teleconnections (e.g., Pacific/North American, North Atlantic Oscillation, and El Nino Southern Oscillation) is compared to the relative influence of monthly and seasonal estimates of precipitation (PRISM, 2014). Previous research has shown that continental-scale teleconnections (e.g., Pacific/North American Pattern, North Atlantic Oscillation, and El Nino Southern Oscillation) are the main drivers of inter-annual variability in temperature and precipitation in the eastern United States (Ropelewski and Halpert, 1986; Hartley, 1999; Henderson and Robinson, 1994). In light of these findings, we hypothesized that the majority of the inter-annual variation in stormflow will be explained by fluctuations in continental-scale teleconnections.

This research determined: (1) the amount of variance that is explained by climate, basin morphology, and land use/land cover; (2) whether soil parent material-specific percentages of land cover explain more variance than generalized watershed-scale percentages, and (3) the role of continental-scale teleconnections and land cover during periods of wetness/dryness. This work was motivated by the need to better understand the drivers of hydrologic variation in meso-scale montane watersheds.

2. Study area

The geology of the SBRM consists of a northeast-trending middle Proterozoic granitic gneiss core that is unconformably overlain on each flank by younger Proterozoic and early Paleozoic quartz diorite and

biotite gneiss with scattered pockets of amphibolite (Robinson et al., 1992). Overlying the bedrock is a thick mantle (up to 30 m) of highly weathered residuum (Southworth et al., 2003). This residuum contributes significant quantities of fine sediment to the valley bottoms through colluvial and fluvial transport processes (Price and Leigh, 2006). The geomorphology of the region is dominated by colluvial processes in the headwaters (Phillips, 2002) and alluvial/colluvial fans mixing with the dominantly fluvial, higher-order alluvial bottomlands (Leigh, 2010; McDonald and Leigh, 2014).

Although elevations are typically higher in the northern and northeastern portion of the SBRM, mean annual rainfall generally decreases from the southwest to the northeast due to orographic lifting and rain-out effects as storm systems move from the Ridge and Valley and Piedmont into the highlands of the SBRM (Fig. 1). Regionally, interactions between oceanic and continental air masses bring frontal systems during winter and tropical disturbances during late summer and early fall (Lecce, 2000). The frequency and character of winter precipitation events in the southeastern US has been shown to correlate with continental-scale teleconnections, including the Pacific North American pattern (PNA) (Leathers et al., 1991; Henderson and Robinson, 1994), the North Atlantic Oscillation (NAO) (Hurrell and Van Loon, 1997; Greenland, 2001), and the El Nino Southern Oscillation (ENSO) (Ropelewski and Halpert, 1986; Eichler and Higgins, 2006).

Non-indigenous settlement of the Southern Blue Ridge Mountains began with small numbers of Euro-American settlers in the late 18th century (Yarnell, 1998). Near the end of the 19th century, forestry and mining became important economic pursuits that greatly affected the region. Near complete deforestation of hillslopes along with poor land use practices (e.g., farming against contours on steep slopes) caused widespread erosion and degradation of the landscape (Glenn, 1911). Eroded sediments from the hillslopes were deposited in the broad flat river valleys resulting in a 1 to 2 m thick stratigraphic deposit of historical alluvium that covers the pre-settlement landscape (Leigh, 2010, 2016). With the introduction of soil conservation programs in the 1930s and a reduction in timber harvest (Yarnell, 1998), sediment loadings were drastically reduced and new floodplains have begun to develop as streams laterally erode into the historical stratum (Leigh, 2010; Rogers and Leigh, 2013).

Regional settlement patterns concentrated almost exclusively on the terraces and bottomlands of the alluvial valleys until the 1960s. Beginning in the 1970s, the number of steep slope, exurban developments began steadily increasing (Gragson and Bolstad, 2006). Population forecasts suggest that many exurban developments will grow to suburban or urban densities within the next twenty years, and up to 67% of new buildings will be built within forested areas (Kirk et al., 2012). While the influences that traditional land use and exurbanization have on water quality and baseflow have been studied (Sutherland et al., 2002; Price et al., 2011; Webster et al., 2012), their influence on stormflow has not yet been examined.

3. Data and methods

3.1. Selection of USGS gages

Out of the approximately 250 USGS-gaged watersheds in the SBRM, 15 watersheds were selected (Fig. 1) that met the following criteria: (1) drainage areas between 30 and 800 km^2 (to target non-headwater, wadeable streams); (2) lacked large impoundments (that would attenuate flood peaks); and (3) had near-continuous (at least 15 complete winter seasons) daily discharge data from 1986–2006. Table 1 is a list of the independent (climatic, geomorphic, and land cover) variables and dependent (hydrologic) variables used in this analysis. Data sources and the methods used to process the data are described in detail below.

3.2. Climate

Analysis intentionally focused on the winter months (December through March) because of the relatively uniform spatial distribution of precipitation that frontal systems have on the SBRM during this season. Due to the regional focus of this study and because each watershed did not have a climate station, monthly PRISM (Parameter-elevation Relationships on Independent Slopes Model) data from the Oregon Climate Group were used to obtain monthly and seasonal estimates of precipitation for each watershed (PRISM, 2014). These monthly estimates of precipitation were determined using a watershed area-weighted average from the 4 km PRISM dataset (Table 1). Indices of the North Atlantic Oscillation (NAO), Pacific/North American pattern (PNA), and El Nino/Southern Oscillation (ENSO) were downloaded from the National Weather Service's Climate Prediction Center (http://www.cpc.ncep.noaa.gov/). These three indices were chosen because previous research found a strong relationship between these three indices and inter-annual variations in temperature and precipitation in the eastern United States.

Henderson and Robinson (1994) found that during a positive PNA, upper-level meridional flows tended to reduce the number of precipitation events but was also often related to relatively large events when they did happen. Their study also found that during a negative PNA, upper-level zonal flows tended to bring more precipitation events but these events are often more clustered and smaller. Conversely, NAO has been found to be positively correlated with temperature and precipitation in the southeastern US (Hartley, 1999). This positive correlation is caused by an increased zonal pressure gradient across the northern Atlantic creating conditions where warmer, wetter air advects into the eastern US (Hurrell and Dickson, 2004). Ropelewski and Halpert (1986) found that in the southeastern United States, the majority of El Nino (La Nina) events were associated with lower (higher) temperatures and higher (lower) amounts of precipitation. These temperature and precipitation differences are likely caused by a displacement of storm tracks eastward or westward during El Nino or La Nina events, respectively (Eichler and Higgins, 2006).

The teleconnection indices were classified by water year (Oct. 1 – Sept. 30) and winter season means were calculated and included as additional independent variables. In order to determine how NAO, PNA, and ENSO affects the inter-monthly character of precipitation in the region, daily precipitation records were obtained from the available long-term climate stations in the region that had mostly complete records from 1986 to 2006 (Fig. 1). For each climate station, total seasonal precipitation and number of peaks were calculated using base R (R Core Team, 2017). Peaks were defined as any peak in daily precipitation that was larger than the day before as well as the day after. Storms were separated using the DataCombine package in R (Gandrund, 2016). The DataCombine package separates periods of precipitation from quiescent periods. Storms were defined as any period of precipitation. The contribution of the largest storm to total precipitation was analyzed by dividing the largest storm of the winter season by total seasonal precipitation during that season (% Max Storm of Total).

Periods of wetness/dryness were subdivided based on z-scores of regional average total winter precipitation. Z-scores were used to determine climatic periods rather than one of the Palmer drought indices because z-scores provide a short-term indicator of wetness or dryness tailored to the data. Using the PRISM dataset, total seasonal precipitation was calculated for each winter season (1986–2006) for each watershed. A regional average of total winter precipitation for the 15 watersheds was used to calculate the z-scores. Years with a z-score between 0.5 and −0.5 were defined as average years, scores exceeding 0.5 were defined as wet years, and scores below −0.5 were defined as dry years. The z-scores for the individual basins agree with the z-scores calculated from the study area averaged winter precipitation totals (Fig. 2). All dry and wet years are consistently dry or wet (with a few average values) across all of the sites.

Table 1
Dependent (stormflow) and independent (climate, geomorphology, and land use/land cover) variables used to determine the drivers of winter (December through March) stormflow.

Hydrology	Abbrev.	Unit	Method/data used to calculate
Ratio of daily peak to 15-minute peak discharge	$Peak_{DAILY}$	–	Flashiness of the peak winter discharge (seasonal maximum daily average discharge divided by the seasonal maximum 15 min discharge)
Richards Baker flashiness index	RBi	–	Daily amount of change or flashiness of winter discharge (sum of the absolute value of daily change in discharge divided by the total amount of discharge)
Stormflow index	Sfi	–	Relative amount of winter stormflow (total stormflow divided by total discharge)
Average peak flow to baseflow ratio	PB_{avg}	–	Average flashiness of winter stormflow peaks (average of stormflow peaks divided by baseflow)
Maximum peak flow to baseflow ratio	PB_{MAX}	–	Flashiness of the peak winter stormflow event (maximum stormflow peak divided by baseflow)
Climate	Abbrev.	Unit	Method/data used to calculate
Total seasonal precipitation	$Precip_{TOTAL}$	mm	Sum of winter (Dec. through Mar.) area-weighted average of monthly PRISM precipitation data
Precipitation during the month of peak discharge	$Precip_{PEAK}$	mm	Area-weighted average of PRISM precipitation data for the month of peak discharge
Precipitation in the month prior to peak discharge	$Precip_{PRIOR}$	mm	Area-weighted average of PRISM precipitation data for the month prior to peak discharge
Precipitation of month prior to and month of peak discharge	$Precip_{SUM}$	mm	Area-weighted average of PRISM precipitation data for the month of and prior to peak discharge
PNA – Month/Season	x_PNA	–	Monthly indices of PNA downloaded from NWS Climate Prediction Center. December (D), January (J), February (F), March (M), and Winter (W).
NAO – Month/Season	x_NAO	–	Monthly indices of NAO downloaded from NWS Climate Prediction Center. December (D), January (J), February (F), March (M), and Winter (W).
ENSO – Months/Season	x_ENSO	–	Three month averaged indices of ENSO downloaded from NWS Climate Prediction Center. Nov.-Jan. (NDJ), Dec.-Feb. (DJF), Jan.-Mar. (JFM), Feb.-Apr. (FMA), Dec.-Mar. (DJFM).
Geomorphology	Abbrev.	Unit	Method/data used to calculate
Drainage area	DA	km^2	Area draining to the gaging station
Total stream length	TSL	km	Using a 4 ha accumulation threshold, total length of streams in the watershed
Entire stream gradient	ESG	%	Along the mainstem, (elevation at 85% stream length – elevation at 15% stream length)/(stream length between 85% and 15%)
Drainage density	DD	km^{-1}	Total stream length/drainage area
Basin length	BL	km	Measured from the headwater divide to the outlet (USGS gage)
Drainage shape	DS	–	Drainage area/(basin length)^2
Average slope	$Slope_{AVG}$	%	Average slope of the watershed determined using a 10 m DEM
Standard deviation of slope	$Slope_{SD}$	%	Standard deviation of the slope of the watershed determined using a 10 m DEM
Average topographic index	$Topo_{AVG}$		Watershed average (ln(area/tan slope)) determined using a 10 m DEM
Standard deviation of the topographic index	$Topo_{SD}$		Watershed standard deviation of (ln(area/tan slope)) determined using a 10 m DEM
Percent 1st order streams	%1st	%	Length of first order streams/total stream length
Standard deviation of elevation	Z_{SD}	km	Standard deviation of the elevation of the watershed
Basin relief	BR	km	Maximum elevation – minimum elevation
Basin relief ratio	BRR	–	Basin relief/basin length
Ruggedness number	RN	–	Basin relief/drainage density
Melton ruggedness ratio	MRR	–	Basin relief/(drainage area)$^{-0.5}$
Hyposmetric index	HI	–	(Mean elevation-minimum elevation)/(maximum elevation – minimum elevation)
Land Use/Land Cover	Abbrev.	Unit	Method/data used to calculate
Road	Road	%	Fraction of watershed covered by roads as estimated with TIGER road coverage. Underscore AC indicates alluvium/colluvium and underscore R indicates residuum.
Grass	Grass	%	Fraction of watershed covered by classes 71 and 81. Underscore AC indicates alluvium/colluvium and underscore R indicates residuum.
Forest	Forest	%	Fraction of watershed covered by classes 41, 42, and 43. Underscore AC indicates alluvium/colluvium and underscore R indicates residuum.
Developed	Dev	%	Fraction of watershed covered by roads and classes 21, 22, 23, and 24. Underscore AC indicates alluvium/colluvium and underscore R indicates residuum.

3.3. Basin characteristics

Basin characteristics used in this analysis describe the size, shape, slope, and relief of the study watersheds and were chosen to represent the variables that were most likely to influence baseflow, stormflow, and/or peak flow (Table 1). All of the basin characteristics were calculated using ArcGIS 10.4, the Spatial Analyst toolbox, and the National Elevation Dataset's 10 m digital elevation model. Stream networks were generated in ArcGIS using the hydrology tools in the spatial analyst toolbox with a flow accumulation threshold of 4 ha (Benstead and Leigh, 2012). Analysis of the initial regression results indicated that only ten of the basin characteristics explain a significant amount of the variance in the dependent hydrologic variables. Table 2 compares these ten geomorphic variables across the 15 watersheds.

Due to county- and state-level differences in soil survey mapping resolution and soil definition criteria (SSURGO soils database; Soil Survey Staff, 2015), parent material was modeled and standardized following the method of McDonald and Leigh (2014). This method delineates probable areas of alluvial or colluvial deposition utilizing slope (0-30°, which is representative of alluvial and colluvial deposits in the study area) and the relative proximity of each pixel to ridgelines or streams. Residuum was assumed to cover the remainder of the study watersheds. While there are bedrock outcrops in the study area, the methods used to delineate the parent material classes could not reliably predict their occurrence. Though locally important, the regional importance of bare rock was deemed minor to non-existent because coverage was less than 1% of the study area (with a maximum watershed coverage of ~4%). Alluvium and colluvium were analyzed together to represent areas that are either perennially or ephemerally connected to the stream network. Residuum was included to represent the hilltops and hillslopes that are not traditionally thought of as being connected to the stream network (though, ephemeral flow paths likely exist).

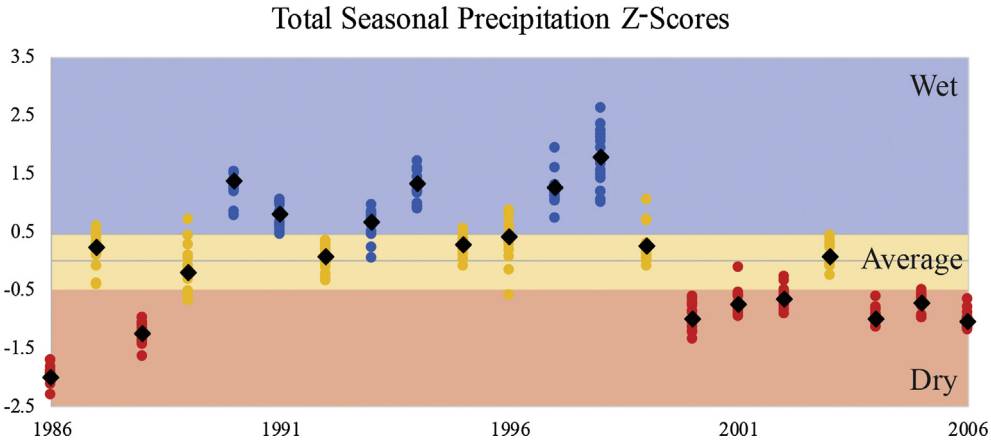

Fig. 2. Z-scores of total winter precipitation for the 15 watersheds and for the regional average (black diamond). Climatic periods are color-coded (dry = red, average = orange, and wet = blue). (For interpretation of the references to color in this figure legend, the reader is referred to the web version of this article.)

3.4. Land use/land cover

Land use/land cover (LULC) data for the years 1986, 1991, 1996, 2001, and 2006 were obtained from the Coweeta (CWT) Long Term Ecological Research program (Hepinstall-Cymerman, 2011). These 30 m resolution datasets classified Landsat imagery according to the National Land Cover Database (NLCD) twenty class system. For this analysis, these twenty classes were generalized into three classes: (1) Forest (classes 41–43); (2) Grass (classes 71 and 81); and (3) Developed (classes 21–24). Land cover percentage estimates for the intervening years were determined by linear interpolation. In order to determine the potential error that linear interpolation may introduce, the known land cover percentages for 1991, 1996, and 2001 were modeled by linearly interpolating between the known years that bracketed them. The average difference between observed (CWT dataset) and modeled LULC was less than ± 1.5% with a maximum error of +6.7% forest in 1991 (McDonald, 2017). Though land cover change often is episodic and nonlinear, this method was determined to be sufficiently robust for this analysis and the errors were below accepted NLCD standards (Wickman et al., 2010). Though row-crop agriculture can have a significant influence on runoff (Knox, 2001), it was not included in this analysis because it covers less than 1% of the study area (Hepinstall-Cymerman, 2011).

Each year's road network was created in ArcGIS by converting the developed pixels (classes 21–24) of each LULC raster to polygons to select intersecting roads from the TIGER (Topologically Integrated Geographic Encoding and Reference) 2010 streets dataset (Trainor et al., 2012). Each year's road network was added to the previous year's network to help control for possible land cover misclassification errors and because roads are not ephemeral features on the landscape. The 2010 TIGER streets dataset was used because there was not a road dataset available for each year that land cover was available, and this dataset was the first to update and correct the road coverage with ground-verified GPS-corrected observations. Streets in this dataset are classified based on route type (RTTYP); which include, U.S. highways (type U), state roads (type S), and smaller roads (types C (county), M (municipal), and O (other)). Aerial photos were used to estimate the widths of each RTTYP. These widths (U = 30 m, S = 15 m, and all other classes = 10 m) were used to buffer the lines and provide an estimate of each watershed covered by roads. All of the land cover types were then converted to polygons and each year's roads were merged with the land cover dataset so that watershed-scale percentages of land cover as well as alluvial/colluvial (AC) and residuum (R) coverages could be subset in ArcGIS and included in the analysis as independent variables (Table 1).

3.5. Hydrology (dependent variables)

Five stormflow variables describing the flashiness (total and relative to base flow) and total amount of stormflow were calculated using the daily average and 15-minute instantaneous discharge records from the USGS. The variables used in this analysis were the ratio between seasonal maximum daily average discharge and the 15-minute maximum discharge ($Peak_{DAILY}$), the Richards Baker flashiness index (RBi, Baker et al., 2004), the stormflow index (Sfi), the average peak flow to baseflow ratio (PB_{AVG}), and the seasonal maximum peak flow to

Table 2
Comparisons of the basin geomorphology of the fifteen USGS watersheds that were used in this analysis. ID corresponds to the watershed labels on Fig. 1.

USGS Gage	ID	DA	ESG	DS	$Slope_{AVG}$	$Slope_{SD}$	$Topo_{SD}$	DD	BRR	MRR	zSD
W. Fork Pigeon River Above Lake Logan, NC (03455500)	1	73	0.079	0.53	24.07	9.26	1.84	2.93	0.09	0.12	0.14
Davidson River Near Brevard, NC (03441000)	2	105	0.050	0.66	22.26	9.62	2.01	3.17	0.09	0.11	0.12
South Toe River Near Celo, NC (03463300)	3	112	0.039	0.42	21.84	9.87	1.93	3.07	0.08	0.12	0.18
Cataloochee Creek near Cataloochee, NC (03460000)	4	127	0.028	0.60	24.44	8.20	1.92	3.07	0.08	0.10	0.14
E. Fork Pigeon River near Canton, NC (03456500)	5	133	0.037	0.29	23.43	9.50	1.96	3.14	0.05	0.09	0.15
Nantahala River near Rainbow Springs, NC (03504000)	6	135	0.012	0.39	21.00	8.13	1.99	3.11	0.04	0.06	0.08
Cartoogechaye Creek near Franklin, NC (03500240)	7	146	0.011	0.46	20.61	10.13	2.15	3.38	0.06	0.09	0.13
Tallulah River near Clayton, GA (02178400)	8	152	0.044	0.63	22.26	9.07	2.07	3.23	0.07	0.09	0.13
Mills River near Mills River, NC (03446000)	9	172	0.032	0.54	20.66	9.14	2.07	3.25	0.06	0.07	0.11
French Broad River at Rosman, NC (03439000)	10	177	0.021	0.40	19.19	9.09	2.09	3.14	0.06	0.09	0.11
Valley River at Tomotla, NC (03550000)	11	268	0.009	0.34	23.37	11.58	2.29	3.50	0.04	0.07	0.12
Little Tennessee River near Prentiss, NC (03500000)	12	362	0.003	0.56	18.22	10.06	2.19	3.39	0.04	0.05	0.11
Oconaluftee River at Birdtown, NC (03512000)	13	477	0.031	0.62	26.01	9.38	2.02	3.24	0.05	0.06	0.18
Chattooga River near Clayton, GA (02177000)	14	525	0.013	0.37	18.27	8.98	2.11	3.27	0.03	0.05	0.13
French Broad River at Blantyre, NC (03443000)	15	766	0.004	0.71	16.58	9.76	2.30	3.40	0.04	0.04	0.22

Table 3
Pearson correlation coefficients (r) describing the strength of the relationship between winter precipitation (daily precipitation) and continental-scale teleconnections (NAO, PNA, and ENSO). Values that are bold and underlined have a p-value < 0.001. Values that are not bold have p-values > 0.05.

Atmospheric Circulation Pattern	Period	Total Precipitation	Number of Peaks	% Max Storm of Total
North Atlantic Oscillation (NAO)	December	**−0.18**	−0.13	**0.22**
	January	−0.10	−0.09	−0.02
	February	**0.18**	**0.27**	**−0.14**
	March	**0.18**	0.06	**0.15**
	Winter	0.04	0.04	**0.12**
Pacific/North American Pattern (PNA)	December	**−0.24**	**−0.43**	**0.22**
	January	**−0.09**	−0.03	**0.21**
	February	**−0.23**	−0.02	**0.12**
	March	−0.05	**−0.28**	**0.12**
	Winter	**−0.25**	**−0.33**	**0.27**
El Nino/Southern Oscillation (ENSO)	Nov.-Jan.	**0.23**	−0.05	**0.25**
	Dec.-Feb.	**0.26**	−0.05	**0.24**
	Jan.-Mar.	**0.28**	−0.05	**0.22**
	Feb.-Apr.	**0.31**	−0.05	**0.20**
	Nov.-Mar.	**0.27**	−0.05	**0.23**

baseflow ratio (PB_{MAX}) (Table 1).

The ratio between seasonal maximum daily average discharge and the 15-minute maximum discharge for that same day ($Peak_{DAILY}$) was calculated as a measure of peak flashiness and to test the possibility that the order of magnitude difference between the study watersheds (70–750 km^2) would influence the rest of the analyses. A high $Peak_{DAILY}$ indicates that the daily average peak is comparable to the 15-minute peak (less flashy). Total seasonal flashiness was calculated using the Richards Baker flashiness index (RBi). RBi is a measure of the daily change or flashiness of flow and is calculated by dividing the sum of the absolute value of daily change in discharge by the total amount of discharge during that period (Baker et al., 2004). A high RBi indicates that the hydrography is very flashy with high peaks and steep rising and falling limbs.

Daily average discharge records were separated into baseflow and stormflow components using the method of Lyne and Hollick (1979). This method uses a recursive digital filter to separate the flow record into quick (stormflow) and slow (baseflow) response components. A forward pass filter is used to separate the quick and slow flow components and a backward pass filter is used to nullify any phase distortion introduced by the forward filter. A filter parameter of 0.805 was used because it provided the best visual fit. Stormflow was calculated by subtracting baseflow from daily average discharge.

The stormflow index (Sfi) was calculated by dividing the total amount of winter stormflow by total winter discharge (the inverse of the more commonly used baseflow index). The average peak flow to baseflow ratio (PB_{AVG}) was calculated by taking the seasonal average of the ratio between peak flow and baseflow. The maximum peak flow to baseflow ratio (PB_{MAX}) is the ratio of seasonal maximum peak flow to baseflow on the day of seasonal maximum peak flow. PB_{AVG} and PB_{MAX} were analyzed to take into account antecedent moisture conditions (baseflow) and provide dimensionless descriptors of peak flow. Due to the relatively coarse temporal resolution of the PRISM dataset (monthly totals), all daily peaks in discharge were included in the analyses regardless of magnitude.

3.6. Statistics

Multiple regression was used to determine the amount of variance in the hydrologic variables that could be explained by the climatic variables and the geomorphic and land cover characteristics of the 15 gaged watersheds. While the gages were chosen due to their consistency and length of record, five of the gages had one or more month missing during the period of study and a total of 18 observations (watershed winters) had to be removed from the initial dataset of 315 watershed winters (15 watersheds times 21 years). In order to determine all of the characteristics that may be influencing regional stormflow, instead of using forward or backward stepwise regression, all possible models containing uncorrelated variables ($|r| < 0.65$) were created and the top three models for each time period for each hydrologic variable are presented below. To understand how periods of wetness/dryness influence the drivers of stormflow, separate models were created for all- (n = 297), average- (n = 99), dry- (n = 114), and wet-years (n = 84). Models were constrained to three variables, because though there were a large number of observations (n of 84–297) only 15 unique watersheds were analyzed. The 'best' models were chosen based on the r^2, p value, F ratio, and AICc characteristics of the model compared to similar models. Prior to creating the regression models, the dependent variables were log_{10} transformed to create normal distributions more suited for parametric statistics.

4. Results

4.1. Continental-scale teleconnections and precipitation

All three teleconnections are weakly to moderately correlated to precipitation in the study area (Table 3). Positive NAO is weakly related to more precipitation and more peaks. This positive correlation between NAO and precipitation agrees with Hartley (1999) and Greenland (2001). Negative PNA is correlated to higher precipitation and more peaks compared to positive PNA (Table 3). Alternatively, during positive PNA the largest storm will be a larger percent of total precipitation than during negative PNA. These results are similar to the findings of Henderson and Robinson (1994) that found positive PNA often had fewer precipitation events but much larger events when they did occur. Interestingly, ENSO has the most consistent and strongest relationship to total precipitation and percent max storm is of the total (Table 3). These results agree with previous research by Ropelewski and Halpert (1986) that found El Nino (warm ENSO-events) to be related to more rainfall in the southern United States. The correlation analysis indicates continental-scale teleconnections can provide an understanding of the character of seasonal rainfall (peak-characteristics) that monthly and seasonal PRISM data cannot provide.

4.2. Daily average peak to 15-minute peak ($Peak_{DAILY}$)

For the time period analyzed, $Peak_{DAILY}$ ranged from 0.21 to 0.99 with a mean of 0.59 (Fig. 3). The smaller watersheds tended to be flashier than the larger watersheds (as expected) and there was very little difference between average-, dry-, and wet-years. The top three $Peak_{DAILY}$ models for each time period are presented in Table 4. For all four time periods, geomorphic differences between the study watersheds (entire stream gradient and relative relief) explain the majority of the explained variance in $Peak_{DAILY}$. A land cover variable explains a significant amount of the explained variance in average- and dry-years. Winter and January PNA along with February and March NAO explain a significant amount of the explained variance during all time periods. A PRISM variable only explains a significant amount of the variance in one model (Table 4).

4.3. Richards Baker flashiness index (RBi)

The RBi values ranged from 0.11 to 0.47 with a mean of 0.24 (Fig. 3). The larger study watersheds tended to be less flashy than the smaller watersheds and dry years less flashy than wet years. The top three RBi models for each time period are presented in Table 5. For all four time periods, geomorphic differences between the study watersheds (standard deviation of the topographic index with the standard

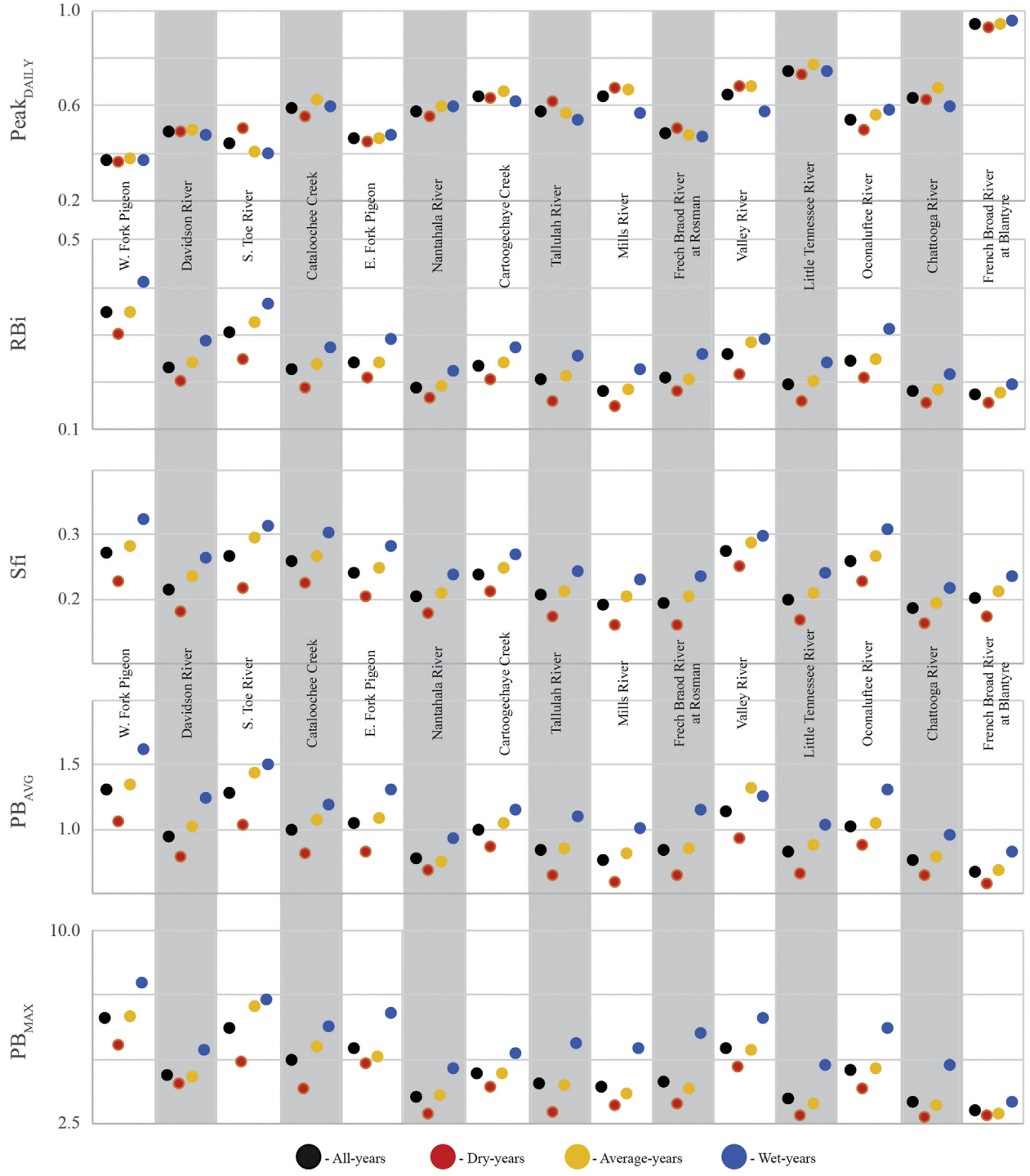

Fig. 3. Comparisons between the mean values of the five dependent hydrologic variables used in this analysis for each of the 15 watersheds. Climatic periods are color-coded (all-years = black, dry = red, average = orange, and wet = blue). (For interpretation of the references to color in this figure legend, the reader is referred to the web version of this article.)

deviation of slope and relative relief) explain the majority of the explained variance in RBi. A land cover variable (roads on alluvium/colluvium) was found to explain a significant amount of the explained variance during average-, dry-, and wet-years. Total winter precipitation explains a significant amount of the explained variance in all of the all-years models. During average-years, PRISM variables (Precipitation – Prior + Peak and Precipitation – Peak) also explain a significant amount of the explained variance in RBi. Alternatively, during dry- and wet-years, NAO and/or PNA explain a significant amount of the explained variance in RBi.

4.4. Stormflow index (Sfi)

Sfi ranged from 0.10 to 0.39 with an average of 0.23 (Fig. 3). Smaller watersheds tended to have higher Sfi than larger watersheds and wet years produced more stormflow than dry years. The top three Sfi models for each time period are presented in Table 6. The majority of the explained variance in all but one of the Sfi models is explained by

Table 4
Models explaining the variance in log-transformed daily average discharge peak to 15-minute instantaneous peak ratio ($Peak_{daily}$). Coefficients (Coeff) and intercepts are from the three variable models.

All-years	Coeff	partial r^2	model r^2	F	AIC	**Average-years**	Coeff	partial r^2	model r^2	F	AIC
Entire Stream Gradient	−4.26	–	0.39 (***)	–	−546.31	Entire Stream Gradient	−4.45	–	0.41 (***)	–	−169.80
Drainage Shape	0.35	0.13	0.52 (***)	77.94	−614.00	Drainage Shape	0.37	0.13	0.53 (***)	25.83	−191.21
NAO – February	0.03	0.03	0.55 (***)	18.95	−630.77	NAO – March	0.04	0.05	0.58 (***)	11.66	−200.45
Intercept	−0.32	–	–	–	–	Intercept	−0.32	–	–	–	–
Topo Index – Std. Dev.	0.81	–	0.41 (***)	–	−555.22	Melton Relative Relief	−3.54	–	0.46 (***)	–	−178.47
Slope – Std. Dev.	−0.06	0.09	0.50 (***)	49.29	−599.05	PNA – Winter	−0.07	0.04	0.50 (**)	8.00	−184.22
Precipitation – Peak	−0.09	0.02	0.52 (***)	16.51	−613.55	Precipitation – Peak	−0.16	0.06	0.56 (***)	12.38	−194.13
Intercept	−1.37	–	–	–	–	Intercept	0.20	–	–	–	–
Melton Relative Relief	−2.77	–	0.42 (***)	–	−557.63	Topo Index – Std. Dev.	0.73	–	0.41 (***)	–	−171.25
Drainage Shape	0.26	0.06	0.48 (***)	34.83	−588.46	A/C – Grass	−0.23	0.09	0.50 (***)	16.34	−184.64
A/C – Grass	0.43	0.03	0.51 (***)	21.60	−607.94	NAO – March	0.05	0.06	0.56 (***)	12.90	−195.03
Intercept	−0.18	–	–	–	–	Intercept	−1.74	–	–	–	–
Dry-years	Coeff	partial r^2	model r^2	F	AIC	**Wet-years**	Coeff	partial r^2	model r^2	F	AIC
Entire Stream Gradient	−4.14	–	0.40 (***)	–	−219.95	Entire Stream Gradient	−4.18	–	0.38 (***)	–	−147.46
Drainage Shape	0.30	0.10	0.50 (***)	23.28	−239.51	Drainage Shape	0.40	0.16	0.55 (***)	28.95	−170.92
PNA – Winter	−0.08	0.05	0.55 (***)	12.93	−249.99	PNA – January	−0.06	0.08	0.62 (***)	15.87	−183.86
Intercept	−0.24	–	–	–	–	Intercept	−0.33	–	–	–	–
Drainage Density	0.42	–	0.43 (***)	–	−226.54	Basin Relief Ratio	−4.61	–	0.27 (***)	–	−133.16
Slope – Average	−0.01	0.08	0.51 (***)	17.85	−241.39	Drainage Shape	0.53	0.26	0.53 (***)	45.23	−168.23
PNA – Winter	−0.08	0.05	0.56 (***)	12.64	−251.60	PNA – January	−0.06	0.07	0.60 (***)	13.57	−179.12
Intercept	−1.23	–	–	–	–	Intercept	−0.25	–	–	–	–
Topo Index – Std. Dev.	0.81	–	0.48 (***)	–	−236.29	Melton Relative Relief	−3.36	–	0.44 (***)	–	−155.77
A/C – Roads	−2.80	0.06	0.54 (***)	14.35	−248.00	Drainage Shape	0.28	0.08	0.52 (***)	14.14	−167.08
PNA – Winter	−0.08	0.05	0.59 (***)	13.44	−258.95	PNA – January	−0.06	0.07	0.59 (***)	13.96	−178.33
Intercept	−1.79	–	–	–	–	Intercept	−0.11	–	–	–	–

* model significant at $p < 0.05$, ** significant at $p < 0.01$, *** significant at $p < 0.001$.

average watershed slope. Development on residuum explains a significant amount of the explained variance during all-, average-, and wet-years. During dry-years, grass on alluvium/colluvium explains a significant amount of the explained variance in Sfi. Similar to RBi, total winter precipitation explains a significant amount of the explained variance in all of the all-years Sfi models. For all of the other time periods, NAO and/or PNA explain a significant amount of the explained variance in Sfi.

4.5. Average peak to base ratio (PB_{AVG})

For the time period analyzed, PB_{AVG} ranged from 0.35 to 2.30 and tended to be higher in smaller watersheds (Fig. 3). The top three PB_{AVG} models for each time period are presented in Table 7. Unlike the models for the previous hydrologic variables, a climate variable (total winter precipitation or February NAO) explains the majority of the explained variance in PB_{AVG} during all- and dry-years. During average- and wet-years, relative relief and stand deviation of the topographic index with

Table 5
Models explaining the variance in log-transformed Richards Baker flashiness index (RBi). Coefficients (Coeff) and intercepts are for the three variable models.

All-years	Coeff	partial r^2	model r^2	F	AIC	**Average-years**	Coeff	partial r^2	model r^2	F	AIC
Topo Index – Std. Dev	−0.77	–	0.12 (***)	–	−421.96	Topo Index – Std. Dev.	−0.79	–	0.15 (***)	–	−170.10
Slope – Std. Dev.	0.11	0.25	0.38 (***)	120.22	−521.72	Slope – Std. Dev.	0.12	0.41	0.56 (***)	89.87	−233.34
Precipitation – Total	0.11	0.26	0.64 (***)	214.65	−682.89	Precipitation – Prior + Peak	0.16	0.11	0.67 (***)	31.22	−259.25
Intercept	−0.30	–	–	–	–	Intercept	−0.29	–	–	–	–
Melton Relative Relief	2.88	–	0.24 (***)	–	−465.78	Melton Relative Relief	2.77	–	0.34 (***)	–	−195.94
Precipitation – Total	0.10	0.22	0.47 (***)	123.30	−567.74	Precipitation – Peak	0.15	0.07	0.41 (**)	10.58	−204.11
Slope – Std. Dev.	0.04	0.08	0.55 (***)	54.91	−616.69	Slope – Std. Dev.	0.05	0.14	0.55 (***)	29.97	−229.03
Intercept	−1.52	–	–	–	–	Intercept	−1.44	–	–	–	–
Drainage Area	0.001	–	0.11 (***)	–	−418.61	Melton Relative Relief	3.30	–	0.34 (***)	–	−195.94
Precipitation – Total	0.10	0.19	0.30 (***)	79.97	−488.13	A/C – Roads	2.85	0.09	0.44 (***)	15.56	−208.63
Elevation – Std. Dev.	2.23	0.23	0.53 (***)	142.88	−604.03	Precipitation – Prior + Peak	0.13	0.08	0.51 (***)	15.06	−220.98
Intercept	−1.07	–	–	–	–	Intercept	−1.14	–	–	–	–
Dry-years	Coeff	partial r^2	model r^2	F	AIC	**Wet-years**	Coeff	partial r^2	model r^2	F	AIC
Topo Index – Std. Dev.	−0.68	–	0.14 (***)	–	−190.37	Topo Index – Std. Dev.	−0.72	–	0.21 (***)	–	−141.74
Slope – Std. Dev.	0.09	0.31	0.44 (***)	60.86	−238.06	Slope – Std. Dev.	0.09	0.28	0.49 (***)	44.89	−176.57
NAO – February	0.04	0.11	0.55 (***)	25.71	−259.81	PNA – December	0.04	0.12	0.61 (***)	23.69	−196.10
Intercept	−0.20	–	–	–	–	Intercept	0.10	–	–	–	–
Melton Relative Relief	2.34	–	0.27 (***)	–	−209.39	Melton Relative Relief	2.60	–	0.34 (***)	–	−157.80
NAO – February	0.04	0.10	0.37 (***)	17.31	−223.76	PNA – December	0.05	0.11	0.46 (***)	16.87	−171.49
PNA – March	0.03	0.05	0.41 (**)	8.81	−230.35	PNA – March	−0.04	0.08	0.54 (***)	14.13	−182.89
Intercept	−0.93	–	–	–	–	Intercept	−0.76	–	–	–	–
Melton Relative Relief	2.81	–	0.27 (***)	–	−209.39	Entire Stream Gradient	3.92	–	0.29 (***)	–	−150.74
NAO – February	0.04	0.10	0.37 (***)	17.31	−223.76	PNA – December	0.04	0.12	0.41 (***)	16.95	−164.49
A/C – Roads	2.64	0.09	0.45 (***)	17.66	−238.55	A/C – Roads	3.13	0.09	0.50 (***)	15.17	−176.81
Intercept	−1.03	–	–	–	–	Intercept	−0.75	–	–	–	–

* model significant at $p < 0.05$, ** significant at $p < 0.01$, *** significant at $p < 0.001$.

Table 6
Models explaining the variance in log-transformed stormflow index (Sfi). Coefficients (Coeff) and intercepts are for the three variable models.

All-years	Coeff	partial r^2	model r^2	F	AIC	**Average-years**	Coeff	partial r^2	model r^2	F	AIC
Slope – Average	0.02	–	0.18 (***)	–	−517.89	Slope – Average	0.02	–	0.36 (***)	–	−271.30
Precipitation – Total	0.10	0.22	0.40 (***)	109.76	−610.06	Slope – Std. Dev.	0.03	0.12	0.48 (***)	21.46	−289.10
Elevation – Std. Dev.	0.94	0.07	0.47 (***)	38.73	−644.86	PNA – January	−0.03	0.07	0.54 (***)	13.95	−300.44
Intercept	−1.39	–	–	–	–	Intercept	−1.30	–	–	–	–
Slope – Average	0.02	–	0.18 (***)	–	−517.89	Slope – Average	0.03	–	0.36 (***)	–	−271.30
Precipitation – Total	0.08	0.22	0.40 (***)	109.76	−610.06	R – Development	2.19	0.10	0.46 (***)	17.48	−285.68
NAO – February	0.03	0.05	0.45 (***)	26.25	−633.47	PNA – January	−0.03	0.07	0.53 (***)	14.25	−297.30
Intercept	−1.25	–	–	–	–	Intercept	−1.23	–	–	–	–
Slope – Average	0.03	–	0.18 (***)	–	−517.89	Slope – Std. Dev.	0.07	–	0.10 (**)	–	−237.90
Precipitation – Total	0.09	0.22	0.40 (***)	109.76	−610.06	Topo Index – Std. Dev.	−0.43	0.36	0.46 (***)	63.56	−286.03
R – Development	2.16	0.05	0.45 (***)	24.05	−631.42	NAO – Winter	0.03	0.05	0.52 (**)	10.79	−294.46
Intercept	−1.49	–	–	–	–	Intercept	−0.41	–	–	–	–
Dry-years	Coeff	partial r^2	model r^2	F	AIC	**Wet-years**	Coeff	partial r^2	model r^2	F	AIC
Slope – Average	0.02	–	0.19 (***)	–	−195.39	Slope – Average	0.02	–	0.25 (***)	–	−189.72
NAO – February	0.06	0.22	0.41 (***)	41.62	−229.54	Precipitation – Peak	0.20	0.12	0.37 (***)	14.87	−201.68
Slope – Std. Dev.	0.03	0.06	0.47 (***)	11.59	−238.77	Elevation – Std. Dev.	0.96	0.11	0.48 (***)	16.86	−215.48
Intercept	−1.48	–	–	–	–	Intercept	−1.26	–	–	–	–
Slope – Average	0.02	–	0.19 (***)	–	−195.39	Slope – Average	0.02	–	0.25 (***)	–	−189.72
NAO – February	0.10	0.22	0.41 (***)	41.62	−229.54	PNA – December	0.03	0.16	0.41 (***)	21.43	−207.23
PNA – January	0.08	0.16	0.57 (***)	41.63	−263.94	NAO – December	0.02	0.09	0.50 (***)	14.69	−219.13
Intercept	−1.21	–	–	–	–	Intercept	−0.94	–	–	–	–
Slope – Average	0.03	–	0.19 (***)	–	−195.39	Slope – Average	0.02	–	0.25 (***)	–	−189.72
NAO – February	0.07	0.22	0.41 (***)	41.62	−229.54	PNA – December	0.03	0.16	0.41 (***)	21.43	−207.23
A/C – Grass	0.50	0.07	0.48 (***)	15.11	−242.02	R – Development	1.80	0.05	0.46 (**)	7.33	−212.34
Intercept	−1.33	–	–	–	–	Intercept	−1.13	–	–	–	–

* model significant at $p < 0.05$, ** significant at $p < 0.01$, *** significant at $p < 0.001$.

Table 7
Models explaining the variance in log-transformed average peak flow to base flow ratio (PB_{avg}). Coefficients (Coeff) and intercepts are from the three variable models.

All-years	Coeff	partial r^2	model r^2	F	AIC	**Average-years**	Coeff	partial r^2	model r^2	F	AIC
Topo Index – Std. Dev.	−0.35	–	0.07 (***)	–	−279.64	Slope – Std. Dev.	0.12	–	0.11 (***)	–	−135.57
Precipitation – Total	0.13	0.20	0.27 (***)	81.03	−349.89	Topo Index – Std. Dev.	−0.78	0.40	0.51 (***)	77.82	−192.17
Slope – Std. Dev.	1.07	0.23	0.51 (***)	138.92	−463.08	NAO – January	0.05	0.07	0.58 (***)	16.19	−205.54
Intercept	0.28	–	–	–	–	Intercept	0.41	–	–	–	–
Drainage Area	−0.001	–	0.08 (***)	–	−283.06	Slope – Average	0.03	–	0.27 (***)	–	−154.65
Precipitation – Total	0.13	0.19	0.27 (***)	74.19	−347.83	Slope – Std. Dev.	0.05	0.12	0.39 (***)	19.52	−170.81
Elevation – Std. Dev.	2.25	0.15	0.42 (***)	76.90	−414.98	PNA – December	−0.06	0.07	0.46 (***)	12.08	−180.44
Intercept	−0.51	–	–	–	–	Intercept	−1.05	–	–	–	–
Melton Relative Relief	3.17	–	0.15 (***)	–	−304.93	Melton Relative Relief	3.32	–	0.26 (***)	–	−154.04
Precipitation – Total	0.12	0.21	0.36 (***)	96.86	−387.45	A/C – Roads	3.58	0.12	0.38 (***)	18.30	−169.14
A/C – Roads	3.06	0.06	0.42 (***)	28.59	−413.03	NAO – January	0.04	0.06	0.45 (**)	11.09	−177.86
Intercept	−0.63	–	–	–	–	Intercept	−0.39	–	–	–	–
Dry-years	Coeff	partial r^2	model r^2	F	AIC	**Wet-years**	Coeff	partial r^2	model r^2	F	AIC
Topo Index – Std. Dev.	−0.69	–	0.06 (**)	–	−105.42	Topo Index – Std. Dev.	−0.66	–	0.14 (***)	–	−122.01
NAO – February	0.09	0.22	0.28 (***)	33.68	−133.48	Slope – Std. Dev.	0.08	0.21	0.35 (***)	26.46	−143.55
Slope – Std. Dev.	0.10	0.18	0.46 (***)	36.05	−163.61	PNA – December	0.05	0.19	0.54 (***)	32.55	−169.96
Intercept	0.35	–	–	–	–	Intercept	0.65	–	–	–	–
Slope – Average	0.02	–	0.15 (***)	–	−116.35	Melton Relative Relief	2.49	–	0.25 (***)	–	−133.46
NAO – February	0.11	0.22	0.37 (***)	39.76	−149.10	PNA – December	0.05	0.18	0.44 (***)	26.20	−154.79
PNA – February	−0.09	0.08	0.46 (***)	16.96	−163.26	NAO – December	0.03	0.09	0.53 (***)	15.46	−167.37
Intercept	−0.62	–	–	–	–	Intercept	−0.13	–	–	–	–
Slope – Average	0.03	–	0.15 (***)	–	−116.35	Entire Stream Gradient	3.56	–	0.20 (***)	–	−127.53
NAO – February	0.09	0.22	0.37 (***)	39.76	−149.10	PNA – December	0.05	0.19	0.39 (***)	25.90	−148.63
R – Development	2.34	0.03	0.40 (*)	5.54	−152.52	A/C- Roads	3.05	0.08	0.47 (**)	11.42	−157.57
Intercept	−0.92	–	–	–	–	Intercept	−0.11	–	–	–	–

* model significant at $p < 0.05$, ** significant at $p < 0.01$, *** significant at $p < 0.001$.

standard deviation of slope explain the majority of the explained variance in PB_{AVG}. Roads on alluvium/colluvium was found to explain a significant amount of the variance during all-years, average-years, and wet-years. December PNA was found to be an important part of the average- and wet-years PB_{AVG} models and February NAO explains a significant amount of the explained variance in all three of the dry-years models. A PRISM variable (total winter precipitation) was only found to explain a significant amount of the explained variance in the all-years models.

4.6. Maximum peak to base ratio (PB_{MAX})

For the years analyzed, PB_{MAX} ranged from 1.51 to 14.71 and tended to be greater in smaller watersheds (Fig. 3). Similar to PB_{AVG}, wet years tended to have flashier peaks than dry. The top three models for each time period are presented in Table 8. A geomorphic variable explains the majority of the explained variance in two of the all-years models and all of the average-years models. During dry-years, winter PNA and February NAO explain more of the explained variance than any of the three geomorphic variables that were found to explain a

Table 8
Models explaining the variance in log-transformed maximum peak flow to base flow ratio (PB_{max}). Coefficients (Coeff) and intercepts are for the three variable models.

All-years	Coeff	partial r^2	model r^2	F	AIC	**Average-years**	Coeff	partial r^2	model r^2	F	AIC
Topo Index – Std. Dev.	−0.92	–	0.09 (***)	–	−152.89	Topo Index – Std. Dev.	−1.09	–	0.13 (***)	–	−58.15
Slope – Std. Dev.	0.12	0.14	0.22 (***)	52.10	−199.29	Slope – Std. Dev.	0.13	0.17	0.30 (***)	22.78	−77.06
Precipitation – Total	0.13	0.15	0.37 (***)	70.12	−260.95	Precipitation – Prior + Peak	0.29	0.12	0.42 (***)	18.70	−92.63
Intercept	1.14	–	–	–	–	Intercept	1.27	–	–	–	–
Drainage Area	−0.001	–	0.10 (***)	–	−157.78	Drainage Area	−0.002	–	0.14 (***)	–	−58.73
Precipitation – Total	0.13	0.11	0.21 (***)	39.66	−193.31	Elevation – Std. Dev.	3.39	0.13	0.27 (***)	16.63	−72.38
Elevation – Std. Dev.	2.59	0.13	0.34 (***)	57.24	−244.24	Precipitation – Prior + Peak	0.32	0.13	0.40 (***)	20.88	−89.83
Intercept	0.15	–	–	–	–	Intercept	−0.05	–	–	–	–
Melton Relative Relief	0.41	–	0.16 (***)	–	−177.54	Slope – Average	0.04	–	0.21 (***)	–	−67.40
Precipitation – Total	0.02	0.13	0.29 (***)	52.98	−224.69	Precipitation – Peak	0.38	0.08	0.29 (**)	11.00	−75.97
A/C – Roads	0.77	0.03	0.32 (***)	12.04	−234.59	NAO – December	0.05	0.10	0.39 (***)	15.23	−88.47
Intercept	0.06	–	–	–	–	Intercept	−0.44	–	–	–	–
Dry-years	Coeff	partial r^2	model r^2	F	AIC	**Wet-years**	Coeff	partial r^2	model r^2	F	AIC
Slope – Average	0.03	–	0.13 (***)	–	−67.37	Topo Index – Std. Dev.	−0.75	–	0.15 (***)	–	−88.85
PNA – Winter	0.34	0.18	0.31 (***)	29.43	−92.03	PNA – January	0.14	0.26	0.41 (***)	35.48	−117.16
NAO – February	0.10	0.18	0.50 (***)	39.29	−124.66	Slope – Std. Dev.	0.08	0.14	0.54 (***)	23.90	−136.86
Intercept	−0.26	–	–	–	–	Intercept	1.50	–	–	–	–
Melton Relative Relief	2.93	–	0.14 (***)	–	−68.66	Slope – Average	0.03	–	0.21 (***)	–	−95.65
PNA – Winter	0.33	0.18	0.32 (***)	29.16	−93.10	PNA – Winter	0.23	0.10	0.32 (***)	12.24	−105.27
NAO – February	0.10	0.17	0.49 (***)	36.51	−123.58	PNA – March	−0.09	0.21	0.53 (***)	35.75	−134.04
Intercept	0.13	–	–	–	–	Intercept	0.14	–	–	–	–
Entire Stream Gradient	3.16	–	0.10 (***)	–	−63.07	Entire Stream Gradient	3.29	–	0.17 (***)	–	−90.70
PNA – Winter	0.34	0.19	0.29 (***)	29.06	−87.44	PNA – January	0.14	0.26	0.43 (***)	36.93	−120.05
NAO – February	0.10	0.17	0.45 (***)	33.74	−115.74	Drainage Shape	−0.32	0.07	0.50 (**)	11.01	−128.62
Intercept	0.28	–	–	–	–	Intercept	0.81	–	–	–	–

* model significant at $p < 0.05$, ** significant at $p < 0.01$, *** significant at $p < 0.001$.

significant amount of the explained variance in PB_{MAX}. During wet-years, January PNA explains the majority of the explained variance. Roads on alluvium/colluvium was found to be significant during all-years but only explained a small portion of the explained variance. Similar to the other dependent variables, total winter precipitation explains a significant amount of the explained variance in all-years PB_{MAX}. During average-years, precipitation variables were also found to explain a significant amount of the explained variance in PB_{MAX}.

4.7. Stormflow drivers

The geomorphic variables that appeared most frequently in the models were average slope and the standard deviation of slope, appearing in 10% of all of the models. The relative importance of average slope was greatest during dry-years (16%) while the importance of the standard deviation of slope was greatest during average-years. While not explaining a large portion of any of the hydrologic variables by itself, when coupled with the standard deviation of the topographic index, Melton relief, or average slope, the standard deviation of slope helped explain a significant amount of the explained variance in all of the dependent variables except for Sfi. Similarly, drainage shape was found to be important when coupled with Melton relief or the entire stream gradient (see Fig. 4).

A land cover variable was an important descriptor of variance in all but four of the climatic periods (wet-years $Peak_{DAILY}$, all-years RBi, and average-, dry-, and wet-years PB_{MAX}). The relative importance of the land cover variables are consistent regardless of the climatic period, explaining on average between 6% and 9% of the variance in the dependent variables. The most frequent land cover variable was roads on alluvium/colluvium which appeared in 4% of all of the models as well as in 4% of the models in each climate period. Both development on residuum and grass on alluvium/colluvium appeared in 2% of the models. Though land cover was found to explain a statistically significant amount of the explained variance, none of the land cover variables were watershed-scale measures of land cover.

The PRISM variable that was in the most models was total seasonal precipitation, appearing in 27% of the all-years models. Though total seasonal precipitation explained a significant amount of the variance in almost all of the all-years models, total seasonal precipitation was not found to explain a significant amount of the variance in any of the other climatic periods. The other two PRISM variables that were found to be important were precipitation during the month of peak discharge and precipitation during the month prior to and during the month of peak discharge. These variables were most important during average-years, appearing in at least one model for each one of the hydrologic variables.

The continental-scale teleconnection that appeared in the most models was February NAO, which appeared in 8% of the models and 27% of the dry-years models. The next most important teleconnections were December and January PNA. These variables appeared in 5% and 4% of the models and 18% and 11% of the wet-years models, respectively. Overall, PNA appeared in slightly more models than NAO (16% versus 13%). In the majority of the models, both NAO and PNA are positively correlated with the dependent variable, indicating stormflow and flashiness will be greatest when the positive phases of the two patterns coincide.

5. Discussion

5.1. Watershed geomorphology

It was initially hypothesized that the geomorphic characteristics of the study watersheds (i.e., slope) would explain the majority of the variance in stormflow. The results indicate that the geomorphic differences between the study watersheds explain the majority of the inter-basin (spatial) variance in regional stormflow. These results are similar to a study by Julian and Gardner (2014) that found watershed characteristics become more important than precipitation regime when comparing larger (> 3rd order) watersheds. Additionally, the results of this study indicate that the importance of each geomorphic variable are dependent variable- and climatic period-specific.

The standard deviation of the topographic index and Melton relief explain the majority of the explained variance in RBi and average slope explains the majority of the explained variance in Sfi and PB_{MAX}. All three of these geomorphic variables explain a significant portion of the

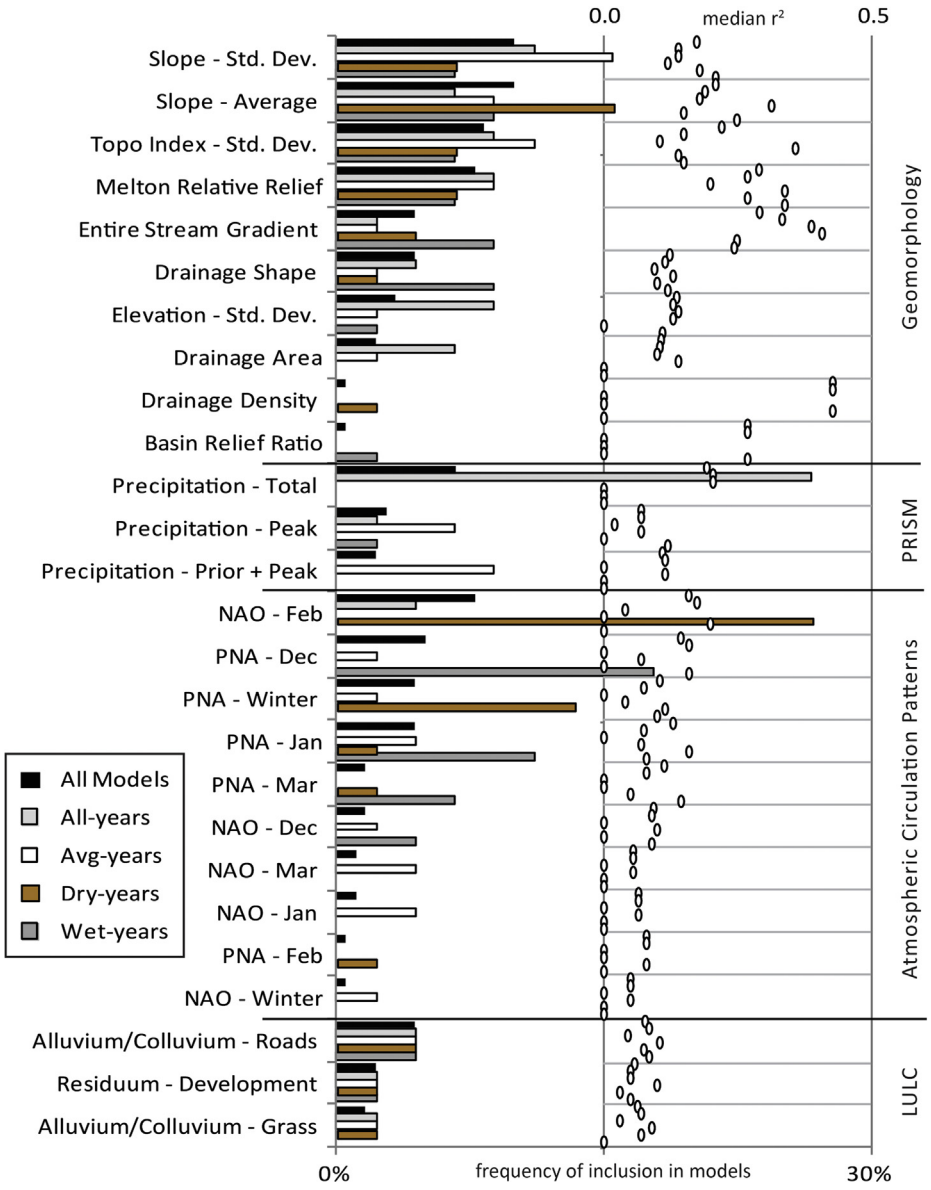

Fig. 4. The bar graph shows the relative frequency of the statistically significant variables from all sixty three-variable models and the inset scatter gram depicts the median magnitude of the r^2 of each variable during each time period.

explained variance in PB_{AVG}, but their importance changes depending on whether the season is dry or wet (Table 7). These findings are similar to those of Sidle et al. (1995) who found antecedent moisture conditions to influence the stormflow response of forested watersheds near Hitachi Ohta, Japan. During dry conditions, Sidle et al. (1995) found that areas connected to the stream network were contributing the majority of stormflow to the streams; while during wet years, hillslopes became the main contributor. The shifting importance of Melton relief and average slope indicates that there also may be a wetness threshold in the SBRM where watershed characteristics that influence the flashiness of stormflow (Melton relief) are influencing peak flows during average- and wet-years and watershed characteristics that favor runoff (average slope) are influencing peak flow during dry-years. Another interpretation is that the wetness threshold may not be related to where the runoff is coming from but the relationship between runoff and baseflow (Zecharias and Brutsaert, 1988). Zecharias and Brutsaert (1988) found average watershed slope to be positively correlated with and a significant predictor of groundwater outflow. During dry-years, the importance of average slope may indicate that there is likely a reduction in baseflow that would cause a relative increase in the average peak flow to baseflow ratio.

$Peak_{DAILY}$ is influenced by the entire stream gradient, drainage shape, and the standard deviation of the topographic index. The influence drainage shape has on $Peak_{DAILY}$ is not surprising and agrees with earlier literature studying flood wave propagation (Gregory and Walling, 1973). The importance of the entire stream gradient and the standard deviation of the topographic index is more complex and is likely related to their relationships to drainage density (McDonald, 2017). Regionally, drainage density is negatively correlated with entire stream gradient and positively correlated with the standard deviation of the topographic index. The importance of the entire stream gradient and the standard deviation of the topographic index and their correlations with drainage density suggest that peak discharge will be flashier in watersheds where drainage density is low. These findings are contrary to previous research that has found a positive relationship between drainage density and peak flow (Carlston, 1963; Gregory and Walling, 1968).

The negative relationship between drainage density and relative relief is not novel to the SBRM and a similar relationship has been found in the mountains of Japan (Oguchi, 1997) and through experimental

methods by Tucker and Bras (1998). Oguchi (1997) concluded that the negative correlation between drainage density and relative relief was due to the influence shallow landslides have on headwater areas of watersheds. Though, studies of debris-flows in the SBRM have found a relatively short recurrence interval for debris flows if the whole region is taken into account (Wieczorek et al., 2000; Eaton et al., 2003), the negative relationship between drainage density and relief is likely due to the saturation threshold theory for channel initiation posited by Tucker and Bras (1998). The steep hillslopes and relatively flat valley bottoms that characterize the Southern Blue Ridge Mountains will quickly transfer subsurface flow through the relatively thick saprolite found on the hillslopes to the relatively flat valley bottoms. The saturation threshold for channel initiation will not be exceeded until the subsurface flow reaches the relatively flat valley bottoms thus imposing a limit on drainage density as hypothesized by Montgomery and Dietrich (1989). The results of this analysis indicate that in humid mountainous regions (i.e., Japan and the SBRM), high drainage density may not always be positively correlated with high flood peaks due to a reduction in drainage density in smaller (flashier) watersheds due to either mass wasting near headwater streams (Japan) or due to a saturation threshold for stream channel initiation in the Southern Blue Ridge Mountains.

Total seasonal flashiness (RBi) is influenced by the standard deviation of the topographic index, Melton relief, and the standard deviation of slope. The influence of these variables is interpreted as Melton relief contributing to the flashiness of the large events (due to its influence on peak flashiness) and the standard deviation of the topographic index and the standard deviation of slope describing the connectedness of hillslope runoff to the stream network. While flashiness tends to decrease with increasing drainage area (Baker et al., 2004), the importance of the Melton relief suggests that, at least in mountainous areas, relative relief is a more important driver of flashiness than just the amount of land draining to the outlet. These results are significant because the studies that utilize RBi often do not include geomorphic variables (besides drainage area) in their models (e.g., Poff et al., 2006; Dow, 2007) and attribute differences in RBi solely to the impact of land cover. While land cover is likely influencing the flashiness of the streams in these studies, the geomorphology of those basins could also be having a significant influence that is completely overlooked.

The importance of average slope (appearing in 10% of the models) is not surprising and is likely related to the infiltration and storage potential of the landscape, similar to the findings of Hewlitt and Hibbert (1967). A study of the relationship between soil and geomorphology in the eastern SBRM found a strong negative correlation between soil thickness and slope (Graham et al., 1990). These conditions would favor runoff over infiltration in steep watersheds, which agrees with the results of this analysis. Additionally, during dry-years when infiltration rates and capacity are likely more important, average slope explains a significant amount of the explained variance in PB_{AVG}. These findings indicate that the characteristics of peak runoff may be related to an infiltration threshold, above which the connectedness of the landscape becomes more important than infiltration rates and capacity.

5.2. Land use/land cover

It was initially hypothesized that development and grasslands in the alluvial bottomlands would have the most influence on stormflow during dry-years. The results indicate that roads and grasslands in the alluvial bottomlands do influence stormflow in the region during all time periods and not just during dry-years. Interestingly, anthropic development on residuum was also found to be an important driver of Sfi during all of the climate periods except for dry-years. The importance of development on residuum is interpreted as a measure of the connectedness of the landscape during average-years (Jones et al., 2000). These results show the importance of understanding the whole watershed and determining whether all of the areas that produce runoff are connected to the stream network. The importance of roads on alluvium/colluvium in the $Peak_{DAILY}$, RBi, and PB_{AVG} models indicate that the relatively small area that is covered by roads in the alluvial and colluvial bottomlands is influencing the flashiness of discharge in the region; agreeing with the effective impervious area of Booth et al. (2002). However, the importance of development on residuum paints a more complex picture of storm runoff and highlights the importance of the increased connectedness of the landscape caused by development (in this case exurbanization) outside of the stream network.

The influence of the other important land cover variable (grass on alluvium/colluvium) on $Peak_{DAILY}$ and Sfi could be due to the lower infiltration rates in pastures found by Johnson (1952) and Price et al. (2011), though it also could be related to the regional prevalence of drainage ditches in the alluvial and colluvial bottomlands (Glenn, 1911). Glenn's (1911) USGS monograph suggested that drainage ditches be dug across the bottomlands to quickly route storm water away from the arable land and reduce the impact precipitation events had on the region. These drainage ditches are still in use today and similar to the findings of Buchanan et al. (2013) will expedite stormflow from the surrounding landscape to the rivers and streams, increasing the importance of stormflow over baseflow.

5.3. Climate

While the geomorphology and land cover of the study area explain the variance between the watersheds, continental-scale teleconnections were found to explain the majority of the inter-annual variation in the dependent variables. The results of this study agree with previous research that found a significant positive correlation between NAO and precipitation in the southeastern United States (Hurrell and van Loon, 1997; Hartley, 1999). These results are not surprising as the enhanced pressure gradient between the Icelandic Low and the Azores High (that characterizes positive NAO) creates conditions that favor zonal flow across the southeastern United States and increases the availability of warm moist air from the Gulf. Interestingly, with the exception of one model (dry-years PB_{AVG}), PNA was also found to be positively correlated with stormflow in the region.

While these results may seem to be contrary to previous research that suggests that the meridional flow that characterizes positive PNA should increase the frequency of blocking events and reduce precipitation in the region (Leathers et al., 1991; Henderson and Robinson, 1994), it is this increased frequency of blocking events that is interpreted as increasing stormflow in the region. Henderson and Robinson (1994) found a significant reduction in the number of events during positive phases of PNA (meridional flow) but the storms that did occur were often larger than the more frequent storms that occurred during negative phases of PNA (zonal flow). These storm event characteristics would explain the increased flashiness caused by positive phases of PNA in the SBRM. Additionally, with a reduction in the number of storms, baseflow will potentially be reduced which will further increase the ratio of stormflow to baseflow when potentially larger storms are affecting the region.

6. Conclusion

The stormflow characteristics (flashiness and magnitude) of fifteen USGS-gaged watersheds in the SBRM were analyzed to determine the drivers of regional stormflow. Forty-five variables describing the geomorphic, climatic, and land cover characteristics of these gaged basins were used to create multiple regression models describing the amount of variance that could be explained in five stormflow variables: peak flashiness ($Peak_{DAILY}$), total flashiness (RBi), relative amount of stormflow (Sfi), average peak flashiness (PB_{AVG}), and maximum peak flashiness (PB_{MAX}). Out of the thousands of potential three variable models, sixty 'best' models were chosen to determine the geomorphic, climatic, and land cover variables that best describe the variance in

regional stormflow during all-, average-, dry-, and wet-years.

Results indicate that watershed geomorphology by itself explains 40–50% of the inter-basin variance in the dependent stormflow variables. Melton relief (basin relief divided by the square root of drainage area) and the standard deviation of the topographic index were found to be the main geomorphic drivers of RBi and average slope was found to be the main geomorphic driver of Sfi and PB_{AVG}. Though drainage area explains a statistically significant amount of the variation in regional stormflow, the importance of Melton relief, the standard deviation of the topographic index, and slope (both watershed average and standard deviation) indicates that the processes controlling stormflow creation and propagation are much more complex than just the size of the watershed. Additionally, this study found that the climate and basin characteristics that explain variance in the hydrologic variables during periods of wetness and drought are significantly different.

By segregating average-, dry-, and wet-years, the influence of low infiltration rate/capacity land cover types could be seen in the average- and dry-years models when the high infiltration rate/capacity areas, that cover the majority of the landscape (forested lands), are not as actively contributing to runoff. The only land cover variables (roads, development, and grassland) that were found to be important were those that cover spatially discrete (on alluvium/colluvium or residuum) areas of the study area. These findings indicate that variance in regional stormflow can not only be explained by land cover near the stream network (on alluvium/colluvium) but also by land cover far from the stream network (on saprolite/residuum).

While the geomorphology of the study area explained much of the variance between the watersheds, continental-scale teleconnections were found to explain the majority of the inter-annual variation in the dependent variables. The results of this study agree with previous research that found a significant positive correlation between NAO and precipitation in the southeastern United States (Hurrell and van Loon, 1997; Hartley, 1999). An interesting finding is that in the majority of the models, PNA was also found to be positively correlated with stormflow in the region.

Though these results may seem to be contrary to previous research that suggests that the meridional flow that characterizes positive PNA should increase the frequency of blocking events and reduce total precipitation in the region, it is this increased frequency of blocking events that is interpreted as increasing stormflow in the region. With a reduction in the number of storms (due to an increased number of blocking events), baseflow will potentially be reduced which will increase the relative importance of stormflow when the potentially larger storms associated with positive PNA do occur. The results of this study highlight the complexity of Southern Blue Ridge Mountain stormflow hydrology and provide a framework from which watershed-scale characteristics can be connected to regional- and continental-scale processes.

Acknowledgements

We would like to acknowledge the UGA physical geography writing group and Drs. Porinchu, Brook, and Garrison for reading early versions of this manuscript. This work was supported by NSF grants DEB-9632854 and DEB-0218001 to the Coweeta LTER.

References

Alberti, M., Booth, D., Hill, K., Coburn, B., Avolio, C., Coe, S., Spirandelli, D., 2007. The impact of urban patterns on aquatic ecosystems: an empirical analysis in Puget lowland sub-basins. Landscape Urban Plann. 80, 345–361.

Baker, D.B., Richards, R.P., Loftus, T.T., Kramer, J.W., 2004. A new flashiness index: characteristics and applications to midwestern rivers and streams. J. Am. Water Resour. Assoc. 40 (2), 503–522.

Benstead, J.P., Leigh, D.S., 2012. An expanded role for river networks. Nature Geoscience 5 (10), 678–679.

Booth, D.B., Hartley, D., Jackson, R., 2002. Forest cover, impervious-surface area, and the mitigation of stormwater impacts. J. Am. Water Resour. Assoc. 38, 835–845.

Bracken, L.J., Croke, J., 2007. The concept of hydrological connectivity and its contribution to understanding runoff-dominated geomorphic systems. Hydrol. Processes 21 (13), 1749–1763.

Buchanan, B.P., Falbo, K., Scheider, R.L., Easton, Z.M., Walter, M.T., 2013. Hydrological impact of roadside ditches in an agricultural watershed in Central New York: implications for non-point source pollutant transport. Hydrol. Processes 27 (17), 2422–2437.

Carle, M.V., Halpin, P.N., Stow, C.A., 2005. Patterns of watershed urbanization and impacts on water quality. J. Am. Water Resour. Assoc. 41, 693–708.

Carlston, C.W., 1963. Drainage Density and Streamflow. United States Geological Survey Professional Paper 422-C.

Chin, A., 2005. Urban transformation of river landscapes in a global context. Geomorphlogy 79 (3), 460–487.

Crowder, B.M., 1987. Economic costs of reservoir sedimentation: a regional approach to estimating cropland erosion damage. J. Soil Water Conserv. 42 (3), 194–197.

Dow, C.L., 2007. Assessing regional land-use/cover influences on New Jersey Pinelands streamflow through hydrograph analysis. Hydrol. Process. 21, 185–197.

Eaton, L.S., Morgan, B.A., Kochel, R.C., Howard, A.D., 2003. Role of debris flows in long-term landscape denudation in the central Appalachians of Virginia. Geology 31, 339–342.

Eichler, T., Higgins, W., 2006. Climatology and ENSO-related variability of North American extratropical cycle activity. J. Clim. 94, 51–65.

Gamble, D.W., Meentemeyer, V.G., 1997. A synoptic climatology of extreme unseasonable floods in the southeastern United States, 1950–1990. Phys. Geogr. 18 (6), 496–524.

Gandrud, C., 2016, DataCombine: tools for easily combining and cleaning data sets. R package version 0.2.21. https://CRAN.R-project.org/package=DataCombine.

Glenn, L., 1911, Denudation and erosion in the southern Appalachian region and Monogahela basin: USGS Professional Paper no. 72, United States Geological Survey, Washington D.C.

Gragson, T.L., Bolstad, P.V., 2006. Land use legacies and the future of southern Appalachia. Soc. Nat. Res. 19 (2), 175–190.

Graham, R.C., Daniels, R.B., Buol, S.W., 1990. Soil-geomorphic relations on the Blue Ridge Front: I. Regolith types and slope processes. Soil Sci. Soc. Am. J. 54 (5), 1362–1367.

Greenland, D., 2001. Multiyear variation of temperature and precipitation in the coastal states of the southeastern United States. Southeastern Geogr. 41, 36–52.

Gregory, K.J., Walling, D.E., 1968. The variation of drainage density within a catchment. Hydrological Sciences Journal 13 (2), 61–68.

Gregory, K.J., Walling, D.E., 1973. Drainage Basins form and Processes: A Geomorphological Approach. Huddersfield, WY, United Kingdom.

Hansen, L., Hellerstein, D., 2007. The value of the reservoir services gained with soil conservation. Land Econ. 83 (3), 285–301.

Hartley, S., 1999. Winter Atlantic climate and snowfall in the south and central Appalachians. Phys. Geogr. 20, 1–13.

Henderson, K.G., Robinson, P.J., 1994. Relationships between the pacific/north american teleconnection patterns and precipitation events in the south-eastern USA. Int. J. Climatol. 14, 307–323.

Hepinstall-Cymerman, J., 2011. Southern Appalachia NLCD Landcover: Coweeta LTER File Archive. University of Georgia, Athens, GA.

Hewlett, J.D., Hibbert, A.R., 1967. Factors affecting the response of small watersheds to precipitation in humid areas. For. Hydrol. 275–290.

Hollis, G.E., 1975. The effect of urbanization on floods of different recurrence intervals. Water Resour. Res. 11 (3), 431–435.

Hollis, G.E., 1979. The hydrological effects of man's activity: a UK perspective. In: Hollis, G.E. (Ed.), Man's Impact on the Hydrological Cycle in the United Kingdom. Norwich, UK.

Hurrell, J.W., Dickson, R.R., 2004, Climate variability over the North Atlantic, in: Nils, S. (ed.), Marine ecosystems and climate variation – the North Atlantic, p. 301–326.

Hurrell, J.W., Van Loon, H., 1997. Decadal variations in climate associated with the North Atlantic oscillation. Clim. Change 36, 301–326.

Jackson, C.R., Bahn, R.A., Webster, J.R., 2017. Water quality signals from rural land use and exurbanization in a mountain landscape: What's clear and what's confounded? J. Am. Water Resour. Assoc. 53, 1212–1228.

Jackson, C.R., Bitew, M., Du, E., 2014. When interflow also percolates: downslope travel distances and hillslope process zones. Hydrol. Process. 28, 3195–3200.

Johnson, E.A., 1952. Effect of farm woodland grazing on watershed values in the southern Appalachian mountains. J. Forest. 50 (2), 109–113.

Jones, J.A., Swanson, F.J., Wemple, B.C., Snyder, K.U., 2000. Effects of roads on hydrology, geomorphology, and disturbance patches in stream networks. Conserv. Biol. 14 (1), 76–85.

Julian, J.P., Gardner, R.H., 2014. Land cover effects on runoff patterns in eastern Piedmont (USA) watersheds. Hydrological Processes 28, 1525–1538.

Kirk, R.W., Bolstad, P.V., Manson, S.M., 2012. Spatio-temporal trend analysis of long-term development patterns (1900–2030) in a Southern Appalachian county. Landscape Urban Plann. 104 (1), 47–58.

Knox, J.C., 1977. Human impacts on Wisconsin stream channels. Ann. Assoc. Am. Geogr. 67 (3), 323–342.

Knox, J.C., 2001. Agricultural influence on landscape sensitivity in the Upper Mississippi River Valley. Catena 42 (2–4), 193–224.

Leathers, D.J., Yarnal, B., Palecki, M.A., 1991. The Pacific/North American teleconnection pattern and United States climate.Part I: Regional temperature and precipitation associations. J. Clim. 4, 517–528.

Lecce, S.A., 2000. Spatial variations in the timing of annual floods in the southeastern United States. Journal of Hydrology 235, 151–169.

Leigh, D.S., 2010. Morphology and channel evolution of small streams in the Southern

Blue Ridge Mountains of western North Carolina. Southeastern Geogr. 50 (4), 379–421.
Leigh, D.S., 2016. Multi-millennial record of erosion and fires in the southern Blue Ridge Mountains, USA. In: Greenberg, K., Collins, B. (Eds.), Natural Disturbances and Range of Variation: Type, Frequency, Severity, and Post-disturbance Structure in Central Hardwood Forests. Springer, New York, NY, pp. 167–201.
Lyne, V., Hollick, M., 1979. Stochastic time-variable rainfall-runoff modelling. Inst. Eng. Aust. Nat. Conf. 79 (10).
McDonald, J.M., Leigh, D.S., 2014, The influence of climate and land cover change on flooding in the southern Blue Ridge Mountains: Annual Meeting of the Association of American Geographers, presented April 8th in Tampa Bay, FL.
McDonald, J.M., 2017. Regional- and local-scale drivers of stormflow and channel morphology in the Southern Blue Ridge Mountains (Doctoral dissertation). University of Georgia, pp. 422.
Miller, J.D., Hyeonjun, K., Kjeldsen, T.R., Packman, J., Grebby, S., Dearden, R., 2004. Assessing the impact of urbanization on storm runoff in a peri-urban catchment using historical change in impervious cover. J. Hydrol. 515, 59–70.
Montgomery, D.R., Dietrich, W.E., 1989. Source areas, drainage density, and channel initiation. Water Resour. Res. 25, 1907–1918.
Montgomery, D.R., Dietrich, W.E., 2002. Runoff generation in a steep soil-mantled landscape. Water Resour. Res. 38 (9) p. 7-1-7-8.
Oguchi, T., 1997. Drainage density and relative relief in humid steep mountains with frequent slope failure. Earth Surf. Proc. Land. 22, 107–120.
Phillips, J.D., 2002. Geomorphic impacts of flash flooding in a forested headwater basin. J. Hydrol. 269 (3), 236–250.
Poff, N.L., Bledsoe, B.P., Cuhaciyan, C.O., 2006. Hydrologic variation with land use across the contiguous United States: geomorphic and ecological consequences for stream ecosystems. Geomorphology 79, 264–285.
Price, K., Leigh, D.S., 2006. Morphological and sedimentological responses of streams to human impact in the southern Blue Ridge Mountains, USA. Geomorphology 78, 142–160.
Price, K., Jackson, C.R., Parker, A.J., 2010. Variation of surficial soil hydraulic properties across land uses in the southern Blue Ridge Mountains. North Carolina, USA, Journal of Hydrology 383, 256–268.
Price, K., Jackson, C.R., Parker, A.J., Reitan, T., Dowd, J., Cyterski, M., 2011. Effects of watershed land use and geomorphology on stream low flows during severe drought conditions in the southern Blue Ridge Mountains, Georgia and North Carolina, United States. Water Resour. Res. 47 (2).
PRISM Climate Group, 2014, Historical precipitation dataset: Oregon State University, http://prism.oregonstate.edu, accessed January 2014.
R Core Team, 2017, R: A language and environment for statistical computing: R Foundation for Statistical Computing, Vienna, Austria, https://www.R-project.org/, accessed 20170926.
Robinson, G.R.J., Lesure, F.G., Marlowe, J.I., Foley, N.K., Clark, S.H., 1992, Bedrock geology and mineral resources of the Knoxville 1 degree by 2 degree quadrangle, Tennessee, North Carolina, and South Carolina, in: United States Geological Survey, ed.
Rogers, J.C., Leigh, D.S., 2013. Modeling stream bank erosion in the Southern Blue Ridge Mountains. Phys. Geogr. 34 (4–5), 354–372.
Ropelewski, C.F., Halpert, M.S., 1986. North American precipitation and temperature patterns associated with the El Nino/Southern Oscillation (ENSO). Mon. Weather Rev. 114, 2352–2362.
Rose, S., Peters, N.E., 2001. Effects of urbanization on streamflow in the Atlanta area (Georgia, USA): a comparative hydrological approach. Hydrol. Process. 15 (8), 1441–1457.
Roy, A.H., Freeman, M.C., Freeman, B.J., Wenger, S.J., Ensign, W.E., Meyer, J.L., 2005. Investigating hydrologic alteration as a mechanism of fish assemblage shifts in urbanizing streams. J. North Am. Benthol. Soc. 24 (3), 656–678.
Sidle, R.C., Tsuboyama, Y., Noguchi, S., Hosoda, I., Fujieda, M., Shimizu, T., 1995. Seasonal hydrologic response at various spatial scales in a small forested catchment, Hitachi Ohta, Japan. J. Hydrol. 168 (1–4), 227–250.
Sidle, R.C., Tsuboyama, Y., Noguchi, S., Hosoda, I., Fujieda, M., Shimizu, T., 2000. Stormflow generation in steep forested headwaters: a linked hydrogeomorphic paradigm. Hydrol. Process. 14, 369–385.
Soil Survey Staff Soil survey geographic (SSURGO) database: Natural Resources Conservation Service, United States Department of Agriculture Available online at http://sdmdataaccess.nrcs.usda.gov/ 2015 Accessed 9/20/2015.
Southworth, S., Schultz, A., Denenny, D., Triplett, J., 2003, Surficial geologic map of the great smoky mountains national park region, Tennessee and North Carolina. Open File Report, vol. 03-081., in: United States Geological Survey, ed.
Sutherland, A.B., Meyer, J.L., Gardiner, E.P., 2002. Effects of land cover on sediment regime and fish assemblage structure in four southern Appalachian streams. Freshw. Biol. 47 (9), 1791–1805.
Trainor, T.F., Johnson, A.G., Kalluri, A., Danso, A., Boudriault, G., Godwin, L., Ratcliffe, M.R., Hanks Jr., G.F., Bishop, D., 2012. In: 2010 TIGER/Line Shapefiles Technical Documentation. U.S. Census Bureau, Department of Commerce, Washingtion, D.C., pp. 215.
Tucker, G.E., Bras, R.L., 1998. Hillslope processes, drainage density, and landscape morphology. Water Resour. Res. 34, 2751–2764.
Webster, J.R., Benfield, E.F., Cecala, K.K., Chamblee, J.F., Dehring, C.A., Gragson, T., Cymerman, J.H., Jackson, C.R., Knoepp, J.D., Leigh, D.S., Maerz, J.C., Pringle, C., Valett, H.M., 2012, Water quality and exurbanization in southern Appalachian streams, in: Boon, P.J., Raven, P.J. (Eds.) River Conservation and Management, pp. 91–106.
Wickman, J.D., Stehman, S.V., Fry, J.A., Smith, J.H., Homer, C.G., 2010. Thematic accuracy of the NLCD 2001 land cover for the conterminous United States. Remote Sens. Environ. 114 (6), 1286–1296.
Wieczorek, G.F., Morgan, B.A., Campbell, R.H., 2000. Debris-flow hazards in the Blue Ridge of central Virginia. Environ. Eng. Geosci. 6, 3–23.
Wolman, M.G., 1967. A cycle of erosion and sedimentation in urban river channels. Geografiska Annaler 49A, 385–395.
Wright, D.B., Smith, J.A., Villarini, G., Baeck, M.L., 2012. Hydroclimatology of flash flooding in Atlanta. Water Resour. Res. 48 (4).
Yarnell, S.L., 1998. The Southern Appalachians: A history of the landscape: General Technical Report SRS-18, United States Department of Agriculture-Forest Service. Southern Research Station.
Zecharias, Y.B., Brutsaert, W., 1988. The influence of basin morphology on groundwater outflow. Water Resour. Res. 24, 1645–1650.